The fate of methyl salicylate in the environment and its role as signal in multitrophic interactions

Yangang Ren, Max Mcgillen, Véronique Daële, J. Casas, Abdelwahid S Mellouki

The fate of methyl salicylate in the environment and its role as signal in multitrophic interactions

Yangang Ren [1], Max R. McGillen [1,2], Véronique Daële [1], Jérôme Casas [3], Abdelwahid Mellouki [1]*

Affiliations

1. Institut de Combustion Aérothermique, Réactivité et Environnement, Centre National de la Recherche Scientifique (ICARE-CNRS), Observatoire des Sciences de l'Univers en région Centre (OSUC), CS 50060, 45071 cedex02, Orléans, France
2. Le Studium Loire Valley Institute for Advanced Studies, Orléans 45071, France
3. Institut de Recherche sur la Biologie de l'Insecte, UMR 7261, Université de Tours, 37200, Tours, France

Corresponding author

* mellouki@cnrs-orleans.fr

Abstract

Phytohormones emitted into the atmosphere perform many functions relating to the defence, pollination and competitiveness of plants. To be effective, their atmospheric lifetimes must be sufficient that these signals can be delivered to their numerous recipients.

We investigate the atmospheric loss processes for methyl salicylate (MeSA), a widely emitted plant volatile. Simulation chambers were used to determine gas-phase reaction rates with OH, NO_3, Cl and O_3; photolysis rates; and deposition rates of gas-phase MeSA onto organic aerosols. Room temperature rate coefficients are determined (in units of cm^3 $molecule^{-1}$ s^{-1}) to be $(3.20\pm0.46)\times10^{-12}$, $(4.19\pm0.92)\times10^{-15}$, $(1.65\pm0.44)\times10^{-12}$ and $(3.33\pm2.01)\times10^{-19}$ for the reactions with OH, NO_3, Cl and O_3 respectively. Photolysis is negligible in the actinic range, despite having a large reported near-UV chromophore. Conversely, aerosol uptake can be competitive with oxidation under humid conditions, suggesting that this compound has a high affinity for hydrated surfaces. A total lifetime of gas-phase MeSA of 1–4 days was estimated based on all these loss processes.

The competing sinks of MeSA demonstrate the need to assess lifetimes of semiochemicals holistically, and we gain understanding of how atmospheric sinks influence natural communication channels within complex multitrophic interactions. This approach can be extended to other compounds that play vital roles in ecosystems, such as insect pheromones, which may be similarly affected during atmospheric transport.

Keywords: methyl salicylate (MeSA), atmospheric chemistry, kinetics, simulation chamber, odor aerosol transport, multitrophic interactions, phytohormones

1. Introduction

The emission of biogenic volatile compounds (BVOCs) into the atmosphere by vegetation carries a metabolic cost, but also concomitant benefits. Methyl salicylate (MeSA, methyl 2-hydroxybenzoate) is an example of a phytohormone that is emitted from a broad variety of species. For example, in their review on floral scents, Knudsen et al. (2006) listed 51 families of flowering plants that have been identified as MeSA emitters in the literature, encompassing many of the world's most economically important crops (such as apples, peaches, almonds and strawberries) in addition to many of the floral constituents of natural ecosystems. There are several proposed strategies by which plants can be advantaged through MeSA emission, as defence mechanisms, as an attractant for pollinators and as a method for reducing the local density of competing plants. MeSA has been observed to be involved in the following interactions:

1. Plant-herbivore interactions: MeSA can stimulate systemic acquired resistance (SAR) responses in healthy plant tissues (Park et al., 2007). This triggers salicylic acid production in the heathy tissues of a plant or in neighbouring plants, which primes plant defences against future herbivorous attacks (Thulke and Conrath, 1998). Furthermore, MeSA may act as a repellent towards certain herbivores (Hardie et al., 1994), although it may be difficult to decouple this effect from other deterrents such as SAR.

2. Plant-predator interactions: Several beneficial arthropods, that are known to predate upon herbivorous pests have been found to use the MeSA emissions of herbivore-infested plants in locating their prey (De Boer and Dicke, 2004; James, 2003; James and Price, 2004), thus reducing herbivorous attacks indirectly.

3. Plant-pollinator interactions: MeSA is a common floral scent that can attract pollinating insects (Dudareva et al., 1998; Knudsen et al., 2006; Loughrin et al., 1991), and is therefore an important component of the reproductive cycle in many flowering plants.

4. Plant-plant interactions: MeSA has been found to exhibit allelopathic effects (Bi et al., 2007), which may interfere with other species growth processes and reduce the root growth of neighbouring plants, favouring the emitter in a competition for soil nutrients.

For each of these four strategies, there is an apparent target for the MeSA emission, and efficient transport between the emitter and the recipient is required in order for these signalling chemicals to perform their function, particularly for cases where transport over long distances is necessary. It is therefore logical that the atmospheric lifetime of MeSA is sufficiently long that transport can occur prior to any chemical transformation in the atmosphere.

Enhanced emissions of MeSA may also occur as a consequence of biotic stress factors such as pathogen infection (Jansen et al., 2011; Martini et al., 2016), or abiotic stresses such as wounding, drought, temperature changes or ozone exposure (Chalal et al., 2015; Heiden et al., 1999; Karl et al., 2008). In these cases, there may be no obvious target for the emission of MeSA and this may be an immune response of wounded or diseased plants. Under these circumstances, MeSA emissions can represent a large flux, which can be comparable or even exceed that of monoterpenes (Karl et al., 2008). If these emissions are a response to abiotic stress factors such as drought or temperature swings, then these fluxes could be occurring across the scale of an ecosystem, which, depending on the atmospheric chemistry of MeSA, could have a major impact upon regional air quality.

Besides the biogenic emissions, which are expected to represent the dominant fluxes of MeSA into the atmosphere, several anthropogenic sources of MeSA exist, which could come from washing and cleaning products, disinfectants, air fresheners, polishes, waxes, cosmetics, personal care products and perfumes (European Chemicals Agency, 2020). Such emissions could impact indoor air quality, and knowledge of the oxidation reactions of MeSA is therefore important in assessing this.

The aim of this work is therefore to assess the various ways in which MeSA can interact with the atmospheric environment, which will allow a first assessment of the sensitivity of MeSA as a

phytohormonal signal towards transport in the atmosphere. Furthermore, these data will provide insight into the role that a large MeSA emission could play in regional air pollution.

2. Experimental methods

2.1 Chamber systems:

Two simulation chamber systems were employed in this work. For particle uptake experiments, the HELIOS chamber was used, which has been described elsewhere (Ren et al., 2019, 2017). In brief, HELIOS is a 90 m^3 hemispherical FEP Teflon foil chamber equipped with two Teflon fans installed at the base, which generate flow velocities of 14 m s^{-1} and induce rapid mixing of reactants in approximately 90 seconds. A three-axis ultrasonic anemometer (Delta Ohm, HD 2003) installed in the centre of the chamber was used to determine pressure, temperature and wind speed/ direction. Relative humidity (RH) was controlled using a water spray system, and was monitored using a humidity probe (Vaisala, HMT333). The chamber was cleaned overnight after each experiment with a fast flow (800 L min^{-1}) of zero air supplied by a pure air generation system (AADCO Instruments, Inc., 737 series).

Kinetic and photolysis measurements were conducted in the 7.3 m^3 ICARE-CNRS chamber, described previously (Bernard et al., 2010). This is a FEP Teflon foil chamber of a cuboidal design, equipped with Teflon fans that promote mixing within 1–2 mins. Illumination was provided artificially from lamp output centred at 254 nm (14 × UV-C T-40 L, Viber Lourmat); at 365 nm (24 × UV-A T-40 L, Viber Lourmat); and broad emissions, >300 nm, from sunlight simulating lamps (12 × Ultra-Vitalux 300 W, Osram). A thermocouple (PT-100) and a humidity probe (Vaisala HMT330) measured the temperature and RH.

Both chambers were operated at a slight overpressure to compensate for sample flows and small leaks, which was achieved using a continuous flow of zero air (5–60 L min^{-1}). This led to gradual dilution of the chamber contents. This was quantified using SF_6 as a tracer, which was monitored

throughout the experiments using Bruker Vertex 70 (pathlength: 303 m) and Nicolet 5700 Magna (pathlength: 143 m) Fourier-transform infrared spectrometers coupled with white-type multipass optics for HELIOS and the 7.3 m^3 chamber respectively.

2.2 Organic compound analysis in the gas and particle phases, and aerosol measurements:

Gas-phase MeSA together with several other organic compounds were monitored using a high-resolution proton transfer reaction time-of-flight mass spectrometer (Ionicon Analytik, PTR-ToF-MS 8000) with a hydronium ion (H_3O^+) detection scheme. The pressure and voltage in the PTR-ToF-MS drift tube was maintained at 2.4 mbar and 480 V affording an electric field strength of 99 Td. The sampling flow was 0.1 L min^{-1}, through a 1 m long, ⅛ inch OD PEEK tube heated to 333 K. A high-resolution time-of-flight FIGAERO-ToF-CIMS instrument (Aerodyne Research Inc. and Tofwerk) with an I^- ionization scheme, similar to instruments described elsewhere (Lee et al., 2014; Lopez-Hilfiker et al., 2014), was used to determine concentrations of MeSA in the gas and particle phases. Voltages affecting ion transmission and declustering were optimized to maximize MeSA.I^- signal using the Thuner software (Tofwerk). The sampling protocol was as follows: aerosol samples were collected through a 1 m long, ¼ inch OD straight length of stainless steel tube at a flow rate of 2 L min^{-1} onto a PTFE filter (SKC, Zefluor™ 25 mm, 2 μm) for 20 mins, and were volatilized by slowly ramping the temperature of a 2 L min^{-1} carrier flow of N_2 from 298 to 573 K over 30 mins, which was held at 573 K for 20 mins subsequently, to ensure that the all particulate-phase MeSA had been thoroughly desorbed. Gas-phase samples were taken during the aerosol collection phase, through a 1 m long, ¼ inch OD PFA tube, also at a flow of 2 SLM. Aerosol size distributions were monitored using a single mobility particle sizer and differential mobility analyzer (3080, 3081 and 3085, TSI) coupled with a condensation particle counter (3788, TSI).

2.3 MeSA introduction system:

Because of the low vapor pressure of MeSA, 0.086 Torr at 298 K (Yaws, 2015), it is difficult to introduce into the chamber using the conventional method of impinging a liquid sample into a carrier gas flow, which would require excessive heating of the liquid sample, and could result in pyrolysis and/ or condensation of the sample in transfer lines. Accordingly, the sample was introduced by nebulizing an aqueous MeSA solution with a commercial nebulizer (TSI, Model 3076) and subsequently volatilizing the nebulized droplets in a 1 m long, ¼ inch OD stainless steel tube held at ~373 K. MeSA is only sparingly soluble in water and the aqueous solution was prepared by introducing 250 mg of MeSA into 500 ml of deionized water (18.2 MΩ·cm at 298 K) and continuously stirring the sample at 333 K for 12 hours. The quantity of MeSA introduced into the chamber was calibrated by nebulizing an aqueous MeSA solution containing known concentrations of internal standards (acetone and cyclohexanone) and analysing all three with the PTR-ToF-MS. The major ions attributed to these standards were found to correlate strongly (R^2 = 0.99) with the protonated mass of MeSA [*m*/*z* 153.0551, $C_6H_4(OH)(C(O)OCH_3)H^+$] over the course of several nebulizing steps (see Figure S1) demonstrating that MeSA volatilization is both complete and reproducible. Subsequently, the intensities of these major ions were compared, yielding slopes and conversion factors (CFs), which were used in the following equation to obtain the gas-phase [MeSA].

$$[MeSA]_{gas} = [\text{internal standard}]_{gas} \times CF \quad (1)$$

The concentrations of internal standards in the gas phase were quantified by expanding known volumes of pure sample into the HELIOS chamber.

2.4 Kinetic studies

The rate coefficients of MeSA + OH, NO_3, Cl and O_3 were determined in the 7.3 m^3 chamber through the relative rate method. In these experiments, the temporal decay of MeSA was monitored in the presence of a reference compound for which the absolute rate coefficient is known. By comparing these decays and accounting for other loss process such as dilution and wall loss (k_d), the rate

coefficient (*k*) can be determined using the following equation (Finlayson-Pitts and Pitts, 2000; Ren et al., 2020):

$$\ln\left(\frac{[\mathrm{MeSA}]_0}{[\mathrm{MeSA}]_t}\right) - k_d t = \frac{k_{\mathrm{MeSA}}}{k_{\mathrm{ref}}} \ln\left(\frac{[\mathrm{ref}]_0}{[\mathrm{ref}]_t}\right) - k_d t \quad (2)$$

where $[MeSA]_0$, $[MeSA]_t$ and $[ref]_0$, $[ref]_t$ are the concentrations of MeSA and reference compounds initially and at time t. Therefore, plots of $\ln\left(\frac{[MeSA]_0}{[MeSA]_t}\right) - k_d t$ vs. $\ln\left(\frac{[ref]_0}{[ref]_t}\right) - k_d t$ yields $\frac{k_{MeSA}}{k_{ref}}$, and with knowledge of the reference rate coefficient (k_{ref}), k_{MeSA} can be placed on the absolute scale.

In the OH experiments, OH radicals were produced using the methyl nitrite precursor through the following sequence of reactions:

$CH_3ONO + h\nu\ (\lambda = 365\ nm) \rightarrow CH_3O + NO$ R1

$CH_3O + O_2 \rightarrow HCHO + HO_2$ R2

$HO_2 + NO \rightarrow OH + NO_2$ R3

In the NO_3 experiments, NO_2 was slowly and continuously introduced into the chamber, maintaining $[NO_2]$ at ~1×10^{12} molecule cm^{-3}, under an excess of O_3 (2.5×10^{13} molecule cm^3), producing NO_3 through the following reaction:

$NO_2 + O_3 \rightarrow NO_3 + O_2$ R4

In the Cl experiments, Cl_2 was photolyzed at 365 nm, yielding two chlorine atoms:

$Cl_2 + h\nu\ (\lambda = 365\ nm) \rightarrow 2Cl$ R5

In the O_3 experiments, O_3 was generated from pure O_2 in a discharge ozone generator (Trailgaz).

2.5 Photolysis studies

Photolysis experiments were conducted at atmospheric pressure and 298 K using artificial light sources in the 7.3 m^3 chamber. In these experiments, MeSA was first introduced into the chamber

and left in the dark for two hours to quantify wall loss and dilution, following this the >300 nm lamps were switched on (see Figure S2). Subsequently, the 365 nm lamps were switched on, and then the 254 nm lamps. To minimize temperature fluctuations induced by the lamps, which may perturb wall loss processes, room air was circulated around the chamber walls using fans. Cyclohexane was added to the chamber as a radical scavenger, to minimize the effects of enhanced radical production either from the chamber walls or the photolysis of MeSA itself. Under chamber conditions, loss processes for MeSA were considered as the following:

MeSA + $h\nu$ (λ = 254/365/>300 nm) $\xrightarrow{J}$ products R6

MeSA $\xrightarrow{k_d}$ wall loss + dilution R7

where J is the photolysis rate and k_d is the combined dark loss (wall loss and dilution rate), with the sum of J and k_d representing k_{total}, the overall loss of MeSA with time. Under irradiation, the total decay of MeSA can be formulated as follows:

$$\ln\left(\frac{[\mathrm{MeSA}]_0}{[\mathrm{MeSA}]_t}\right) = k_{\mathrm{total}}t \quad (3)$$

and J is obtained by subtracting the dark loss k_d, obtained at the beginning of the experiment, from k_{total}:

$$J = k_{total} - k_d \quad (4)$$

2.6 Materials:

Methyl salicylate (>99%, TCI), methyl ethyl ketone (99%, Sigma-Aldrich), di-*n*-butyl ether (99.3%, Sigma-aldrich), toluene (>99.5%, TCI), chloroacetone (95%, Alfa Aesar), acetaldehyde (>99.5%, Sigma-Aldrich), benzaldehyde (>99%, Sigma-Aldrich) and 3,3,3-trifluoropropene (99%, Sigma-Aldrich), O_2 (99.999%, Air-Liquide), N_2 (99.999%, Air-Liquide), chlorine (99.6%, Air-Liquide), NO_2 (1% in N_2, Air-Liquide), methanol (99.98%, Biosolve), sodium nitrite (>97%, Sigma-Aldrich), nitric acid

(70%, Sigma-Aldrich), sulphuric acid (95%, Prolabo) and P_2O_5 (≥98%, Fluka) were used as supplied, without further purification. Methyl nitrite was synthesized by adding sulphuric acid (50% in water) dropwise to a saturated solution of sodium nitrite in methanol that was stirred continuously and held at 273 K in a 3-necked flask, the effluent was swept through a water bubbler using a small flow of N_2, to remove water soluble impurities such as HONO, then through a drying tube containing P_2O_5, before entering a cold trap maintained at 77 K. The sample was then purified under vacuum.

3. Results and discussion

3.1 Surface uptake of MeSA

Four types of experiments were conducted in the HELIOS chamber to evaluate the uptake of MeSA under a variety of conditions (see Table 1):

A. Dry (<1%) with no secondary organic aerosol (SOA) present.
B. Dry (<1%) with SOA produced from limonene ozonolysis.
C. Humid (~40–60%) with no SOA present.
D. Humid (~40–60%) with limonene SOA.

Figure S3 presents a typical experimental time profile of MeSA in the presence of humid SOA. The possible loss of MeSA through reaction with O_3 was tested by exposing MeSA to 200 ppb of O_3 over the course of 90–120 minutes. Loss of MeSA was indistinguishable from dilution and can therefore be neglected. Hence, particle deposition rates on SOA and chamber surfaces were determined as follows. Firstly, first-order losses of gas-phase MeSA with respect to SOA and chamber surfaces were calculated thus:

$$k'_{\mathrm{dry}} = k_{\mathrm{total_A}} - k_{\mathrm{SF_6}} = 1.0 \pm 0.1 \times 10^{-6}\mathrm{s}^{-1} \quad (5)$$

$$k'_{\mathrm{dry\,SOA}} = k_{\mathrm{total_B}} - k_{\mathrm{SF_6}} - k'_{\mathrm{dry}} = 0.4 \pm 0.1 \times 10^{-6}\mathrm{s}^{-1} \quad (6)$$

$$k'_{\mathrm{humid}} = k_{\mathrm{total_C}} - k_{\mathrm{SF_6}} = 4.8 \pm 0.1 \times 10^{-6}\mathrm{s}^{-1} \quad (7)$$

$$k'_{\text{humid SOA}} = k_{\text{total}_D} - k_{SF_6} - k'_{\text{humid}} = 2.1 \pm 0.1 \times 10^{-6} s^{-1} \quad (8)$$

where k'_x represent first-order decays of MeSA with respect to dry chamber, humid chamber, dry SOA and humid SOA surfaces (see Figure S4); k_{SF6} is the dilution rate as defined by SF_6 loss, and k_{total} represents the total first-order loss of MeSA observed during the experiment, corresponding to conditions A, B, C and D respectively.

Using these first-order decays, deposition rates can be calculated for chamber and SOA surfaces as follows:

$$k_{\text{chamber}} = \frac{k'_{\text{dry}} \text{ or } k'_{\text{humid}}}{\frac{S_{\text{chamber}}}{V_{\text{chamber}}}} \text{ and } k_{SOA} = \frac{k'_{\text{dry SOA}} \text{ or } k'_{\text{humid SOA}}}{\frac{Sa}{V}} \quad (9)$$

where $S_{chamber}$ and $V_{chamber}$ are the surface area and volume of the chamber, 108 m^2 and 90 m^3 respectively; S_a/V represents the particle surface density calculated from the particle size distribution measured by the SMPS between 3 and 500 nm and assuming a spherical shape (see Figure S3) . Deposition rates were ordered as follows, $k_{\text{dry chamber}}$ (8.3×10^{-7}) < $k_{\text{humid chamber}}$ (4.0×10^{-6}) < $k_{\text{dry SOA}}$ (3.0×10^{-4}) < $k_{\text{humid SOA}}$ (1.8×10^{-3}), with calculated values in parentheses in units of m s^{-1}.

Further experimental details are provided in Table 1. Ultimately, condition D is expected to be the most realistic, since MeSA is emitted from the terrestrial biosphere, likely in the presence of moisture and other BVOCs. However, it was necessary to study the other conditions in order to isolate the effects of humidity and SOA surfaces and chamber surfaces. Different analytical approaches were employed to investigate deposition processes, resulting in three key findings:

1. SMPS measurements show that introduction of gas-phase MeSA slows the decrease of SOA mass concentration over time, indicating that gas-phase MeSA partitions to SOA (see Figure 1).
2. PTR-ToF-MS measurements demonstrate that first-order losses of gas-phase MeSA are enhanced by SOA and humidity (see Table 1), showing that gas-phase MeSA is being lost to surfaces, especially humid surfaces.

3. SOA particles sampled by the CIMS FIGAERO inlet were found to contain MeSA (see Figure 2), corroborating points 1 and 2.

The partitioning fraction of gas-phase MeSA onto SOA (*F*) was defined based on the referece of Pankow (1994) and estimated in two ways of this work. Firstly, the concentration of MeSA lost to SOA surfaces $[\mathrm{MeSA}]_{\mathrm{lost}}$ was quantified using the first-order loss rate for $k'_{\mathrm{dry\ SOA}}$ and $k'_{\mathrm{humid\ SOA}}$ derived from Eqs. 6 and 8 respectively, divided by the concentration of MeSA in the chamber in the presence of SOA particles, $[\mathrm{MeSA}]^{\#}$:

$$F = \frac{[\mathrm{MeSA}]_{\mathrm{lost}}}{[\mathrm{MeSA}]^{\#}} = \frac{[\mathrm{MeSA}]_0\left(1-\exp\left(-k'_{\mathrm{dry\ SOA}}\ or\ -k'_{\mathrm{humid\ SOA}}\times t\right)\right)}{[\mathrm{MeSA}]^{\#}} \quad (10)$$

Secondly, the mass of SOA mass in the presence and absence of gas-phase MeSA was integrated over a time period of ~3 hours as shaded area in Figure 1 ($\int_0^t \mathrm{SOA}_{\mathrm{MeSA}}$ and $\int_0^t \mathrm{SOA}$, respectively), providing an alternative calculation of *F*:

$$F = \frac{\int_0^t \mathrm{SOA}_{\mathrm{MeSA}} - \int_0^t \mathrm{SOA}}{[\mathrm{MeSA}]^{\#}} \quad (11)$$

Equation 10 yielded values for *F* of 0.2–4.6% under dry and humid conditions respectively, whereas Equation 11 was only employed under humid conditions and resulted in *F* = 10.9%. These findings are therefore in general accordance with previous suggestions that, as a result of its low vapour pressure (Yaws, 2015), under typical aerosol mass loadings of 1–50 μg m^{-3},[26] 0.4–18% of MeSA is expected to partition to the particle phase (Karl et al., 2008), based on partition modelling (Pankow, 1994). It is noted that on the timescales of our experiments, there is insufficient time for equilibrium of gas-phase MeSA with SOA surfaces to be established, which may be a contributory factor in the spread of values provided by Eqs. 10 and 11, and our estimates of partitioning may also be slightly lower than previous estimates would indicate. Furthermore, we find that there is an enhancement of MeSA uptake at humid condition (see Table 1), suggesting that the activity towards MeSA on humid surfaces is higher than that of dry ones, which is an inference that would not emerge from

simple partition models. Molecular modelling work(Liyana-Arachchi et al., 2013) has demonstrated the intuitive result that the oxygenated sites of MeSA have a high affinity for water, which may explain this enhancement, and also shows that once MeSA has entered the particle phase, it will accumulate primarily at the air-water interface.

3.2 Atmospheric oxidation of MeSA

Rate coefficients for the reactions of MeSA with OH, NO_3, Cl and O_3 were determined at room temperature (296±2 K) using the relative rate method. Figure 3 presents the plots of $\ln\left(\frac{[\mathrm{MeSA}]_0}{[\mathrm{MeSA}]_t}\right) - k_d t$ vs. $\ln\left(\frac{[\mathrm{ref}]_0}{[\mathrm{ref}]_t}\right) - k_d t$ yields $\frac{k_{\mathrm{MeSA}}}{k_{\mathrm{ref}}}$ and the obtained $\frac{k_{\mathrm{MeSA}}}{k_{\mathrm{ref}}}$ according to the experiment conditions are shown in Table 2. Reference compound rate coefficients were taken from the recent evaluated database of McGillen et al. (2020) (see Table 2), and were used to place these reactions on the absolute scale. These are as follows, in units of cm^3 $molecule^{-1}$ s^{-1}:

MeSA + OH	→	products	(3.20±0.46) × 10^{-12}	(R8)
MeSA + NO_3	→	products	(4.19±0.92) × 10^{-15}	(R9)
MeSA + Cl	→	products	(1.65±0.44) × 10^{-12}	(R10)
MeSA + O_3	→	products	(3.33±2.01) × 10^{-19}	(R11)

There is one previous experimental study of the kinetics of MeSA oxidation (Canosa-Mas et al., 2002), where the reactions of R10 and R11 were measured. For R10, adjusting for re-evaluation of the reference rate coefficient, Cl + acetone (McGillen et al., 2020), a value of 2.5±0.3 × 10^{-12} cm^3 $molecule^{-1}$ s^{-1} was obtained, which is higher than our value of (1.65±0.44) × 10^{-12}. The same study determined R11 to be >4.1 × 10^{-22}, based on a relative rate with respect to the reaction of O_3 + toluene (Atkinson, 1994), and also provided a rough estimate of ~4 × 10^{-21} cm^3 $molecule^{-1}$ s^{-1} using an absolute method. In our case, we find the rate coefficient of R11 to be (3.33±2.01) × 10^{-19} cm^3 $molecule^{-1}$ s^{-1}, using the relative method, which is considerably larger than the previous

296 determination. The reasons for these discrepancies are unclear, although it is noted that the
297 chamber employed in the previous experiments is substantially smaller (0.05 m^3) than that of this
298 study, and for a compound of low vapour pressure such as MeSA, any wall effects are likely to be
299 exacerbated by a greatly increased surface-area to volume ratio. In relation to R11, it is further
300 noted that the reactivity of O_3 with other closely related oxygenated aromatic compounds such as
301 guaiacol has been found to be quite similar to our determination (Zein et al., 2015), k = (4.0±3.1) ×
302 10^{-19} cm^3 $molecule^{-1}$ s^{-1}, and suggests that phenolic compounds such as these have an enhanced
303 reactivity compared with other aromatics.

304 We present the first determinations for the rate coefficient of R8 and R9. Compared with the
305 reaction of OH + phenol (McGillen et al., 2020), k = 2.80 × 10^{-11} cm^3 $molecule^{-1}$ s^{-1}, k_{R8} is almost an
306 order of magnitude smaller, suggesting that the acetate group *ortho* with respect to a hydroxyl
307 group has an electron-withdrawing effect on the aromatic ring. This hypothesis is supported by the
308 slow rate of R9 and R10, since each of these reactions is expected to be dominated by electrophilic
309 addition to the ring system. It was observed during test experiments on k_{R9} that much larger rate
310 coefficients were observed at higher [NO_2] (where N_2O_5 was used as the NO_3 source). This is similar
311 to previous findings on NO_3 + alkylnaphthalenes (Phousongphouang and Arey, 2002). This
312 phenomenon can be attributed to an equilibrium complex formed in R9, which may undergo a fast
313 reaction with NO_2. For this reason, [NO_2] was kept at a minimum by maintaining R4 under a large
314 excess of O_3. This suggests that similar precautions should be taken when measuring NO_3 rate
315 coefficients with other aromatic species.

316 k_{R8} can also be compared with structure-activity relationship predictions. Taking the approach of
317 Kwok and Atkinson (1995), a value of 1.1 × 10^{-11} cm^3 $molecule^{-1}$ s^{-1} is predicted, which is considerably
318 larger than our measured value. The likely reason for this is because of the paucity of data regarding
319 aromatics that contain an acetate group. Unfortunately, it appears that the recent technique of
320 Jenkin et al.(2018) is optimized based solely on this estimated value, which is probably unintentional,

and yields an identical value to Kwok and Atkinson.(1995) This comparison highlights the need to study the kinetics of more compounds of this type, which are currently poorly represented in the experimental database (McGillen et al., 2020). Given the large variety of hormonal compounds that are emitted by the biosphere (Herrmann, 2010), and the small number of these compounds whose atmospheric chemical behaviour has been determined experimentally, it is crucial that estimation methods such as these are improved, so that the impact of the environment on semiochemicals can be better assessed.

3.3 Atmospheric photolysis of MeSA

The potential for several UV wavelengths (254/ 365/ >300 nm) to photolyze MeSA was investigated. In the case of the 365 and >300 nm lamps, photolytic loss of MeSA was found to be statistically indistinguishable from the dark losses (see Figure S5, Table S1). For the 254 nm lamps, the photolysis rate was significant ($2.82 \pm 0.26 \times 10^{-5}$ s^{-1}), although this wavelength is not important in the troposphere (Finlayson-Pitts and Pitts, 2000), and is presented here only for completeness.

A previous study determined the UV absorption cross section of MeSA (Canosa-Mas et al., 2002), and found a strong chromophore with a peak of ~1.5×10^{-17} cm^2 $molecule^{-1}$ at 310 nm. Assuming that this measurement is correct, and that the quantum yield of photolysis is unity, this would lead to very significant losses of MeSA in the troposphere and would dominate its overall loss in the atmosphere. However, our measurements suggest the opposite. The reasons for this discrepancy cannot be known with certainty, but two possibilities are considered. Firstly, the cross section could be inaccurate – this was determined by measuring absorbance in the saturated headspace above a pure sample of MeSA. There are several pitfalls to this approach, most notably, that under saturated conditions, it is expected that MeSA could deposit on the absorption cell windows, which could strongly influence the retrieved cross section. Secondly, even with a large absorbance, the photolysis quantum yield could be very low, leading to no measurable transformation of MeSA within the

actinic range. Either way, we conclude that photolysis is not a major sink for MeSA under tropospheric conditions.

3.4 Atmospheric lifetime of MeSA

A practical approach to estimating the importance of atmospheric loss processes is to calculate the lifetime of MeSA with respect to each loss process. Oxidation lifetimes are calculated thus:

$$\tau_{\mathrm{ox}} = \frac{1}{[\mathrm{ox}] \cdot k_{\mathrm{ox}}} \quad (12)$$

where [ox] is a globally representative concentration of a given oxidant in molecule cm^{-3} (see Table 3 for the selected values (Atkinson, 1991; Monks et al., 2009; Spivakovsky et al., 2000; Wingenter et al., 1996)), k_{ox} is the rate coefficient of the reaction of MeSA with respect to that oxidant in cm^3 $molecule^{-1}$ s^{-1}, and τ_{ox} is the lifetime in seconds.

The lifetime with respect to photolysis, τ_{phot}, is provided using an analogous equation:

$$\tau_{\mathrm{phot}} = \frac{1}{\mathrm{J}} \quad (13)$$

The lifetime with respect to heterogeneous loss is considered as follows (Jacob, 1999):

$$\tau_{\mathrm{heterogeneous}} = \left(\frac{1}{\frac{S_a}{V} \cdot k_{\mathrm{dry\ SOA}}} + \frac{1}{\frac{S_a}{V} \cdot k_{\mathrm{humid\ SOA}}} + \frac{1}{\frac{S}{V} k_{\mathrm{dry\ surface}}} + \frac{1}{\frac{S}{V} \cdot k_{\mathrm{humid\ surface}}} \right)^{-1} \quad (14)$$

where S_a represents the SOA surface area S represents the various ground and vegetation surfaces. Typical S_a/V ratios for rural and urban areas range from 10^{-4} to 10^{-3} m^{-1} (Li et al., 2012; Wang et al., 2016), which result in lifetimes between 1 and 190 days and are therefore comparable to gas-phase oxidation.

Once all loss processes have been accounted for, the overall lifetime can be assessed through Equation (15):

$$\frac{1}{\tau_{\mathrm{total}}} = \frac{1}{\tau_{\mathrm{OH}}} + \frac{1}{\tau_{\mathrm{NO_3}}} + \frac{1}{\tau_{\mathrm{O_3}}} + \frac{1}{\tau_{\mathrm{Cl}}} + \frac{1}{\tau_{\mathrm{phot}}} + \frac{1}{\tau_{\mathrm{heterogeneous}}} \quad (15)$$

366 which leads to an estimated total lifetime of gas-phase MeSA of 1–4 days.

367 It should be emphasized that globally averaged values of [ox], J values and *S*/*V* employed in Eq. 15
368 will not always be applicable in understanding the fate of emissions from a terrestrial ecosystem. For
369 example, recent work shows that NO_3 (which is considered on a global scale to be an exclusively
370 night-time oxidant) plays an important role even during the day in some forested environments
371 (Liebmann et al., 2019). Similar caveats are offered regarding the heterogeneous losses described in
372 Eq. 14, where local factors such as the amount and type of vegetation surfaces and the season in
373 which the emission occurred could have a profound effect on the uptake of MeSA and analogous
374 compounds. However, such further, more detailed analyses of these points are beyond the scope of
375 the present study.

376 A further consideration is that the loss of gas-phase MeSA onto SOA surfaces is not necessarily a
377 permanent sink for this compound. The affinity for MeSA towards the air-water interface (Liyana-
378 Arachchi et al., 2013), and our FIGAERO-CIMS measurements, demonstrates the reversibility of
379 MeSA uptake and suggests that MeSA may subsequently re-enter the gas phase under field
380 conditions. It is therefore logical, given that in the absence of surfaces MeSA emissions would be
381 rapidly advected and diluted, that the presence of surfaces – whether they are leaf or aerosol
382 surfaces – could actually slow the removal of MeSA from a local environment. Accordingly, these
383 loss processes are not considered within the lifetime assessment.

384 **4. Atmospheric and ecological implications**

385 Our analysis may help to assess the plausibility of some of the proposed ecological roles of MeSA.
386 For example, its lifetime with respect to oxidation is sufficiently long under field conditions that
387 transport from the point of emission would be possible over 10s of kilometres, which is more than
388 necessary in most cases. Of course, an emission from a single plant would be highly dispersed over
389 this distance, however, a collective emission from an ecosystem, such as that observed by Karl et

al.(2008) could influence the semiochemistry of the air over this region, and may be able to affect the response of an ensemble of plants towards herbivory, systematic acquired resistance or in attracting pollinators and herbivore predators.

By investigating the many diverse sinks of MeSA, it is apparent that both OH and NO_3 represent the dominant permanent sinks, and that losses during the night-time are lower. Given that MeSA along with several other floral scents possess a circadian emission profile, with higher emissions during the night (Loughrin et al., 1991), it is possible to hypothesize that some plants may have adapted their emissions to account for the atmospheric reactivity of MeSA or perhaps other phytohormones. Given that sufficient kinetic information is available for relatively few phytohormones, this hypothesis remains speculative.

The observation that a substantial fraction of MeSA can partition to aerosol particles is consistent with previous studies (Karl et al., 2008; Liyana-Arachchi et al., 2013), and should be an important focus when investigating signalling among biotic entities. Indeed, MeSA is perceived at the same time and location as many other semiochemicals within an odorscape, by a variety of organisms (Conchou et al., 2019; Xu and Turlings, 2018). Here, MeSA can serve the dual role of a synergetic compound with insect pheromones, for example in facilitating the orientation to a sexual partner (Xu and Turlings, 2018), or antagonistically, by hampering this orientation (Rouyar et al., 2015), depending on the volatile, plant and insect species. The efficiency of transport within the atmosphere and the sensory mechanisms by which these compounds operate are so far unknown, but they have already been exploited in pest management programs, for example in combining a crop species with repelling or masking plants (Mofikoya et al., 2019). Like MeSA, other semiochemicals (especially pheromones) with similar physicochemical properties may partition to SOA, which could be instrumental in their atmospheric transport. It is clear that further work is needed, particularly regarding how semiochemicals that are absorbed onto surfaces are perceived by the biota of interest.

Acknowledgments

This work is supported by Labex Voltaire (ANR-10-LABX-100-01), ARD PIVOTS program and PIA PHEROEARO programs (both supported by the Centre-Val de Loire regional council), and the European Union's Horizon 2020 research and innovation programme through the EUROCHAMP-2020 Infrastructure Activity under grant agreement No. 730997. MRM thanks Le Studium for their support over the duration of this project.

References

Atkinson, R., 1994. Gas-phase tropospheric chemistry of organic compounds, Journal of physical and chemical reference data Monograph. American Institute of Physics [u.a.], Woodbury, NY.

Atkinson, R., 1991. Kinetics and Mechanisms of the Gas-Phase Reactions of the NO_3 Radical with Organic Compounds. J. Phys. Chem. Ref. Data 20, 459–507. https://doi.org/10.1063/1.555887

Bernard, F., Eyglunent, G., Daële, V., Mellouki, A., 2010. Kinetics and Products of Gas-Phase Reactions of Ozone with Methyl Methacrylate, Methyl Acrylate, and Ethyl Acrylate. J. Phys. Chem. A 114, 8376–8383. https://doi.org/10.1021/jp104451v

Bi, H.H., Zeng, R.S., Su, L.M., An, M., Luo, S.M., 2007. Rice Allelopathy Induced by Methyl Jasmonate and Methyl Salicylate. J. Chem. Ecol. 33, 1089–1103. https://doi.org/10.1007/s10886-007-9286-1

Canosa-Mas, C.E., Duffy, J.M., King, M.D., Thompson, K.C., Wayne, R.P., 2002. The atmospheric chemistry of methyl salicylate—reactions with atomic chlorine and with ozone. Atmos. Environ. 36, 2201–2205. https://doi.org/10.1016/S1352-2310(02)00173-5

Chalal, M., Winkler, J.B., Gourrat, K., Trouvelot, S., Adrian, M., Schnitzler, J.-P., Jamois, F., Daire, X., 2015. Sesquiterpene volatile organic compounds (VOCs) are markers of elicitation by sulfated laminarine in grapevine. Front. Plant Sci. 6. https://doi.org/10.3389/fpls.2015.00350

Conchou, L., Lucas, P., Meslin, C., Proffit, M., Staudt, M., Renou, M., 2019. Insect Odorscapes: From Plant Volatiles to Natural Olfactory Scenes. Front. Physiol. 10, 972. https://doi.org/10.3389/fphys.2019.00972

De Boer, J.G., Dicke, M., 2004. The Role of Methyl Salicylate in Prey Searching Behavior of the Predatory Mite Phytoseiulus persimilis. J. Chem. Ecol. 30, 255–271. https://doi.org/10.1023/B:JOEC.0000017976.60630.8c

Dudareva, N., Raguso, R.A., Wang, J., Ross, J.R., Pichersky, E., 1998. Floral Scent Production in *Clarkia breweri*: III. Enzymatic Synthesis and Emission of Benzenoid Esters. Plant Physiol. 116, 599–604. https://doi.org/10.1104/pp.116.2.599

European Chemicals Agency, 2020. Substance Infocard - methyl salicylate [WWW Document]. URL https://echa.europa.eu/fr/substance-information/-/substanceinfo/100.003.925 (accessed 2.27.20).

Finlayson-Pitts, B.J., Pitts, J.N., 2000. Chemistry of the upper and lower atmosphere: theory, experiments, and applications. Academic Press, San Diego.

Hardie, J., Isaacs, R., Pickett, J.A., Wadhams, L.J., Woodcock, C.M., 1994. Methyl salicylate and (−)-(1R,5S)-myrtenal are plant-derived repellents for black bean aphid,Aphis fabae Scop. (Homoptera: Aphididae). J. Chem. Ecol. 20, 2847–2855. https://doi.org/10.1007/BF02098393

Heiden, A.C., Hoffmann, T., Kahl, J., Kley, D., Klockow, D., Langebartels, C., Mehlhorn, H., Sandermann, H., Schraudner, M., Schuh, G., Wildt, J., 1999. Emission of volatile organic compounds from ozone-exposed plants. Ecol. Appl. 9, 1160–1167. https://doi.org/10.1890/1051-0761(1999)009[1160:EOVOCF]2.0.CO;2

Herrmann, A., 2010. The chemistry and biology of volatiles. Wiley, Chichester, West Sussex, UK ; [Hoboken, N. J].

Jacob, D.J., 1999. Introduction to atmospheric chemistry. Princeton University Press, Princeton, N.J.

James, D.G., 2003. Synthetic Herbivore-Induced Plant Volatiles as Field Attractants for Beneficial Insects. Environ. Entomol. 32, 977–982. https://doi.org/10.1603/0046-225X-32.5.977

James, D.G., Price, T.S., 2004. Field-Testing of Methyl Salicylate for Recruitment and Retention of Beneficial Insects in Grapes and Hops. J. Chem. Ecol. 30, 1613–1628. https://doi.org/10.1023/B:JOEC.0000042072.18151.6f

Jansen, R.M.C., Wildt, J., Kappers, I.F., Bouwmeester, H.J., Hofstee, J.W., van Henten, E.J., 2011. Detection of Diseased Plants by Analysis of Volatile Organic Compound Emission. Annu. Rev. Phytopathol. 49, 157–174. https://doi.org/10.1146/annurev-phyto-072910-095227

Jenkin, M.E., Valorso, R., Aumont, B., Rickard, A.R., Wallington, T.J., 2018. Estimation of rate coefficients and branching ratios for gas-phase reactions of OH with aromatic organic compounds for use in automated mechanism construction. Atmospheric Chem. Phys. Discuss. 1–37. https://doi.org/10.5194/acp-2018-146

Karl, T., Guenther, A., Turnipseed, A., Patton, E.G., Jardine, K., 2008. Chemical sensing of plant stress at the ecosystem scale. Biogeosciences 5, 1287–1294. https://doi.org/10.5194/bg-5-1287-2008

Knudsen, J.T., Eriksson, R., Gershenzon, J., Ståhl, B., 2006. Diversity and Distribution of Floral Scent. Bot. Rev. 72, 1–120. https://doi.org/10.1663/0006-8101(2006)72[1:DADOFS]2.0.CO;2

Kwok, E., Atkinson, R., 1995. Estimation of hydroxyl radical reaction rate constants for gas-phase organic compounds using a structure-reactivity relationship: An update. Atmos. Environ. 29, 1685–1695. https://doi.org/10.1016/1352-2310(95)00069-B

Lee, B.H., Lopez-Hilfiker, F.D., Mohr, C., Kurtén, T., Worsnop, D.R., Thornton, J.A., 2014. An Iodide-Adduct High-Resolution Time-of-Flight Chemical-Ionization Mass Spectrometer: Application to Atmospheric Inorganic and Organic Compounds. Environ. Sci. Technol. 48, 6309–6317. https://doi.org/10.1021/es500362a

Li, X., Brauers, T., Häseler, R., Bohn, B., Fuchs, H., Hofzumahaus, A., Holland, F., Lou, S., Lu, K.D., Rohrer, F., Hu, M., Zeng, L.M., Zhang, Y.H., Garland, R.M., Su, H., Nowak, A., Wiedensohler, A., Takegawa, N., Shao, M., Wahner, A., 2012. Exploring the atmospheric chemistry of nitrous acid (HONO) at a rural site in Southern China. Atmospheric Chem. Phys. 12, 1497–1513. https://doi.org/10.5194/acp-12-1497-2012

Liebmann, J., Sobanski, N., Schuladen, J., Karu, E., Hellén, H., Hakola, H., Zha, Q., Ehn, M., Riva, M., Heikkinen, L., Williams, J., Fischer, H., Lelieveld, J., Crowley, J.N., 2019. Alkyl nitrates in the boreal forest: formation via the NO_3-, OH- and O_3-induced oxidation of biogenic volatile organic compounds and ambient lifetimes. Atmospheric Chem. Phys. 19, 10391–10403. https://doi.org/10.5194/acp-19-10391-2019

Liyana-Arachchi, T.P., Hansel, A.K., Stevens, C., Ehrenhauser, F.S., Valsaraj, K.T., Hung, F.R., 2013. Molecular Modeling of the Green Leaf Volatile Methyl Salicylate on Atmospheric Air/Water Interfaces. J. Phys. Chem. A 117, 4436–4443. https://doi.org/10.1021/jp4029694

Lopez-Hilfiker, F.D., Mohr, C., Ehn, M., Rubach, F., Kleist, E., Wildt, J., Mentel, Th.F., Lutz, A., Hallquist, M., Worsnop, D., Thornton, J.A., 2014. A novel method for online analysis of gas and particle composition: description and evaluation of a Filter Inlet for Gases and AEROsols (FIGAERO). Atmospheric Meas. Tech. 7, 983–1001. https://doi.org/10.5194/amt-7-983-2014

Loughrin, J.H., Hamilton-Kemp, T.R., Andersen, R.A., Hildebrand, D.F., 1991. Circadian rhythm of volatile emission from flowers of Nicotiana sylvestris and N. suaveolens. Physiol. Plant. 83, 492–496. https://doi.org/10.1111/j.1399-3054.1991.tb00125.x

Martini, X., Willett, D.S., Kuhns, E.H., Stelinski, L.L., 2016. Disruption of Vector Host Preference with Plant Volatiles May Reduce Spread of Insect-Transmitted Plant Pathogens. J. Chem. Ecol. 42, 357–367. https://doi.org/10.1007/s10886-016-0695-x

McGillen, M.R., Carter, W.P.L., Mellouki, A., Orlando, J.J., Picquet-Varrault, B., Wallington, T.J., 2020. Database for the kinetics of the gas-phase atmospheric reactions of organic compounds. Earth Syst. Sci. Data Discuss. Under review. https://doi.org/10.5194/essd-2019-236

Mofikoya, A.O., Bui, T.N.T., Kivimäenpää, M., Holopainen, J.K., Himanen, S.J., Blande, J.D., 2019. Foliar behaviour of biogenic semi-volatiles: potential applications in sustainable pest management. Arthropod-Plant Interact. 13, 193–212. https://doi.org/10.1007/s11829-019-09676-1

Monks, P.S., Granier, C., Fuzzi, S., Stohl, A., Williams, M.L., Akimoto, H., Amann, M., Baklanov, A., Baltensperger, U., Bey, I., Blake, N., Blake, R.S., Carslaw, K., Cooper, O.R., Dentener, F.,

Fowler, D., Fragkou, E., Frost, G.J., Generoso, S., Ginoux, P., Grewe, V., Guenther, A., Hansson, H.C., Henne, S., Hjorth, J., Hofzumahaus, A., Huntrieser, H., Isaksen, I.S.A., Jenkin, M.E., Kaiser, J., Kanakidou, M., Klimont, Z., Kulmala, M., Laj, P., Lawrence, M.G., Lee, J.D., Liousse, C., Maione, M., McFiggans, G., Metzger, A., Mieville, A., Moussiopoulos, N., Orlando, J.J., O'Dowd, C.D., Palmer, P.I., Parrish, D.D., Petzold, A., Platt, U., Pöschl, U., Prévôt, A.S.H., Reeves, C.E., Reimann, S., Rudich, Y., Sellegri, K., Steinbrecher, R., Simpson, D., ten Brink, H., Theloke, J., van der Werf, G.R., Vautard, R., Vestreng, V., Vlachokostas, Ch., von Glasow, R., 2009. Atmospheric composition change – global and regional air quality. Atmos. Environ. 43, 5268–5350. https://doi.org/10.1016/j.atmosenv.2009.08.021

Pankow, J.F., 1994. An absorption model of the gas/aerosol partitioning involved in the formation of secondary organic aerosol. Atmos. Environ. 28, 189–193. https://doi.org/10.1016/1352-2310(94)90094-9

Park, S.-W., Kaimoyo, E., Kumar, D., Mosher, S., Klessig, D.F., 2007. Methyl Salicylate Is a Critical Mobile Signal for Plant Systemic Acquired Resistance. Science 318, 113–116. https://doi.org/10.1126/science.1147113

Phousongphouang, P.T., Arey, J., 2002. Rate Constants for the Gas-Phase Reactions of a Series of Alkylnaphthalenes with the OH Radical. Environ. Sci. Technol. 36, 1947–1952. https://doi.org/10.1021/es011434c

Ren, Y., Bernard, F., Daële, V., Mellouki, A., 2019. Atmospheric Fate and Impact of Perfluorinated Butanone and Pentanone. Environ. Sci. Technol. 53, 8862–8871. https://doi.org/10.1021/acs.est.9b02974

Ren, Y., Grosselin, B., Daële, V., Mellouki, A., 2017. Investigation of the reaction of ozone with isoprene, methacrolein and methyl vinyl ketone using the HELIOS chamber. Faraday Discuss. 200, 289–311. https://doi.org/10.1039/C7FD00014F

Ren, Y., McGillen, M., Ouchen, I., Daële, V., Mellouki, A., 2020. Kinetic and product studies of the reactions of NO3 with a series of unsaturated organic compounds. J. Environ. Sci. S1001074220301030. https://doi.org/10.1016/j.jes.2020.03.022

Robinson, A.L., Donahue, N.M., Shrivastava, M.K., Weitkamp, E.A., Sage, A.M., Grieshop, A.P., Lane, T.E., Pierce, J.R., Pandis, S.N., 2007. Rethinking Organic Aerosols: Semivolatile Emissions and Photochemical Aging. Science 315, 1259–1262. https://doi.org/10.1126/science.1133061

Rouyar, A., Deisig, N., Dupuy, F., Limousin, D., Wycke, M.-A., Renou, M., Anton, S., 2015. Unexpected plant odor responses in a moth pheromone system. Front. Physiol. 6. https://doi.org/10.3389/fphys.2015.00148

Spivakovsky, C.M., Logan, J.A., Montzka, S.A., Balkanski, Y.J., Foreman-Fowler, M., Jones, D.B.A., Horowitz, L.W., Fusco, A.C., Brenninkmeijer, C.A.M., Prather, M.J., Wofsy, S.C., McElroy, M.B., 2000. Three-dimensional climatological distribution of tropospheric OH: Update and evaluation. J. Geophys. Res. Atmospheres 105, 8931–8980. https://doi.org/10.1029/1999JD901006

Thulke, O., Conrath, U., 1998. Salicylic acid has a dual role in the activation of defence-related genes in parsley. Plant J. 14, 35–42. https://doi.org/10.1046/j.1365-313X.1998.00093.x

Wang, G., Zhang, R., Gomez, M.E., Yang, L., Levy Zamora, M., Hu, M., Lin, Y., Peng, J., Guo, S., Meng, J., Li, J., Cheng, C., Hu, T., Ren, Y., Wang, Yuesi, Gao, J., Cao, J., An, Z., Zhou, W., Li, G., Wang, J., Tian, P., Marrero-Ortiz, W., Secrest, J., Du, Z., Zheng, J., Shang, D., Zeng, L., Shao, M., Wang, W., Huang, Y., Wang, Yuan, Zhu, Y., Li, Y., Hu, J., Pan, B., Cai, L., Cheng, Y., Ji, Y., Zhang, F., Rosenfeld, D., Liss, P.S., Duce, R.A., Kolb, C.E., Molina, M.J., 2016. Persistent sulfate formation from London Fog to Chinese haze. Proc. Natl. Acad. Sci. 113, 13630–13635. https://doi.org/10.1073/pnas.1616540113

Wingenter, O.W., Kubo, M.K., Blake, N.J., Smith, T.W., Blake, D.R., Rowland, F.S., 1996. Hydrocarbon and halocarbon measurements as photochemical and dynamical indicators of atmospheric hydroxyl, atomic chlorine, and vertical mixing obtained during Lagrangian flights. J. Geophys. Res. Atmospheres 101, 4331–4340. https://doi.org/10.1029/95JD02457

572 Xu, H., Turlings, T.C.J., 2018. Plant Volatiles as Mate-Finding Cues for Insects. Trends Plant Sci. 23,
573 100–111. https://doi.org/10.1016/j.tplants.2017.11.004
574 Yaws, C.L., 2015. The Yaws Handbook of Vapor Pressure. Elsevier. https://doi.org/10.1016/C2014-0-
575 03590-3
576 Zein, A.E., Coeur, C., Obeid, E., Lauraguais, A., Fagniez, T., 2015. Reaction Kinetics of Catechol (1,2-
577 Benzenediol) and Guaiacol (2-Methoxyphenol) with Ozone. J. Phys. Chem. A 119, 6759–
578 6765. https://doi.org/10.1021/acs.jpca.5b00174
579

580

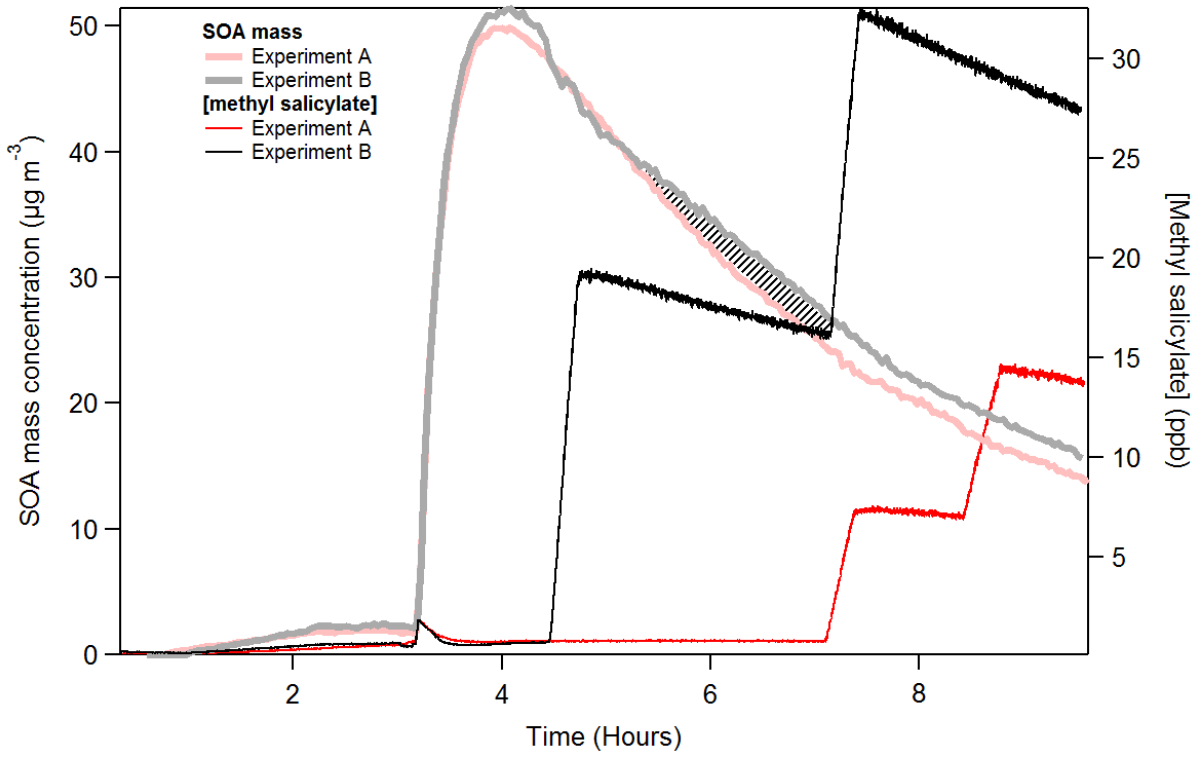

581

582 **Figure 1.** Time profile of secondary organic aerosol (SOA) mass concentration in the absence /
583 presence of MeSA under the condition of RH ca 50%. Experiment A: MeSA introduced when SOA
584 mass concentration ca. 45 µg m^{-3}; Experiment B: MeSA introduced when SOA mass concentration ca.
585 25 µg m^{-3}. A reduction in the rate of SOA mass decrease is observed upon introduction of MeSA,
586 indicating uptake from the gas phase. The shaded area presents the calculation of partitioning
587 fraction of gas-phase MeSA onto SOA (*F*) in Equation 12.

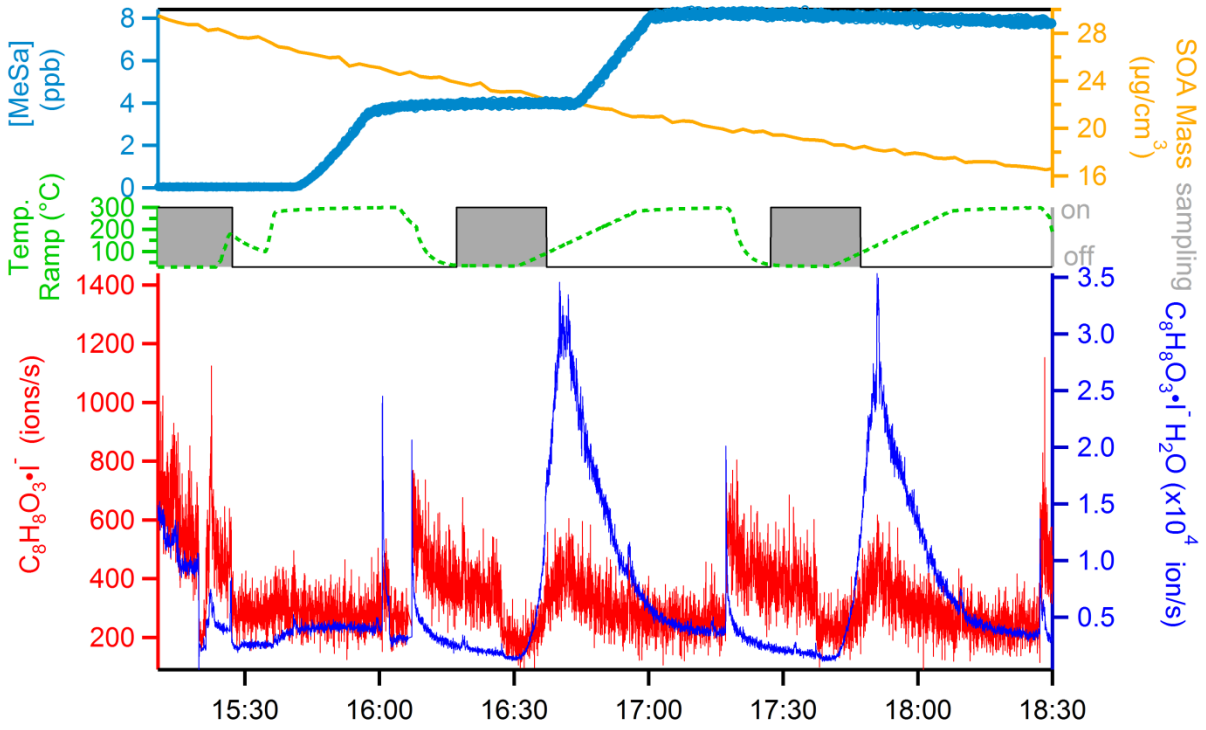

Figure 2. Time series of MeSA under humid conditions (~40-60%) with SOA in HELIOS. Upper Panel: MeSA concentration was quantified using PTR-ToF-MS and SOA mass concentration was calculated from size distribution in the SMPS. Middle Panel: Temperature ramp of on-line SOA composition analysis in FIGAERO-CIMS, the grey-shaded area indicates the gas-phase analysis and SOA sampling in the same time; Lower Panel: the MeSA signal ($C_8H_8O_3I^-$, m/z 278.952 and $C_8H_8O_3I^-•H_2O$, m/z 278.952) in FIGAERO-CIMS.

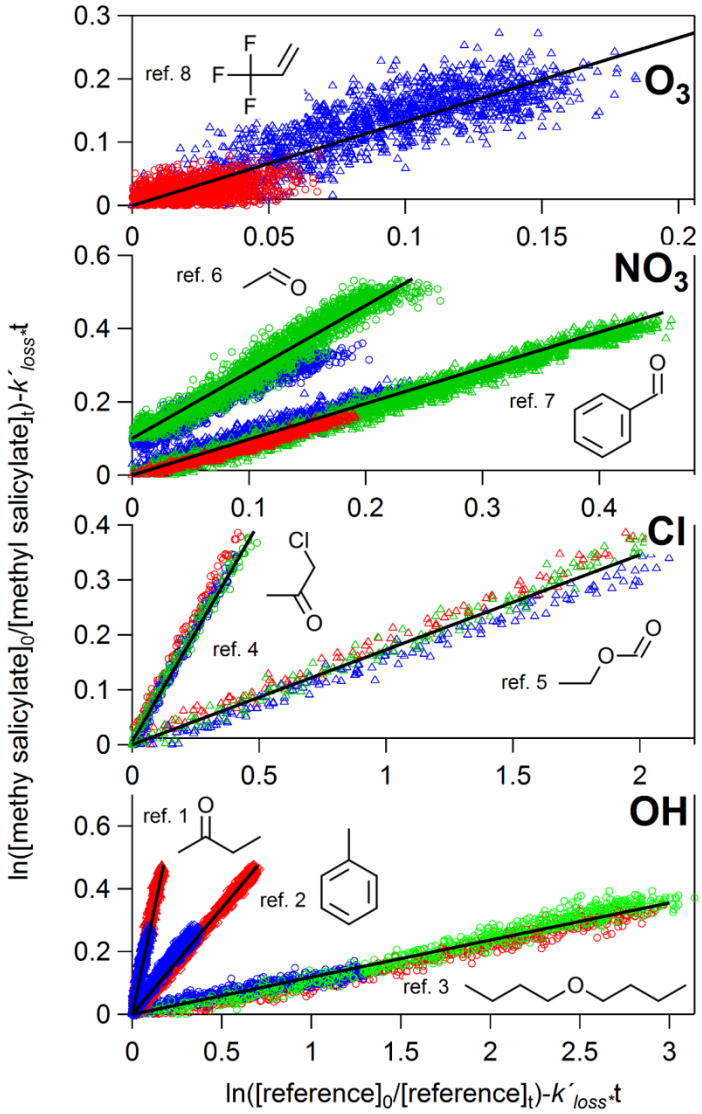

595

596 **Figure 3:** Plots of relative rate kinetic data obtained for the OH, Cl, NO_3 and O_3 reactions with MeSA.
597 Note that each color (blue, green and red) represents individual experiments using the same
598 reference compound. OH references: ref. 1 methyl ethyl ketone, ref. 2 toluene and ref. 3 di-*n*-butyl
599 ether; Cl references: ref. 4 chloroacetone and ref. 5 ethyl formate; NO_3 references: ref. 6
600 acetaldehyde and ref. 7 benzaldehyde; O_3 references: ref. 8 3,3,3-trifluoropropene. Ref. 6 was offset
601 0.1 on the y-axis for clarity.

602

603